Theory and Quantum Dynamics Simulations of Exciton-Polariton Motional Narrowing

Wenxiang Ying,[1,*] M. Elious Mondal,[1] and Pengfei Huo[1,2,†]

[1] *Department of Chemistry, University of Rochester, 120 Trustee Road, Rochester, New York 14627, USA*

[2] *The Institute of Optics, Hajim School of Engineering, University of Rochester, Rochester, New York 14627, USA*

(Dated: June 7, 2024)

The motional narrowing effect has been extensively studied for cavity exciton-polariton systems in recent decades both experimentally and theoretically, which is featured by (1) the subaverage behavior, and (2) the asymmetric linewidths for the upper polariton (UP) and the lower polariton (LP). However, a minimal theoretical model that is clear and adequate to address all these effects, as well as the linewidth scaling relations remains missing. In this work, based on the single mode 1D Holstein-Tavis-Cummings (HTC) model, we studied the motional narrowing effect of the polariton linear absorption (LA) spectra via both semi-analytic derivations and numerically exact quantum dynamics simulations using the hierarchical equations of motion (HEOM) approach. The results reveal that under collective light-matter coupling between a cavity mode and N molecules, the polariton linewidth scales as $1/\sqrt{N}$ under the slow limit, while scales as $1/N$ under the fast limit, due to the polaron decoupling effect. Further, by varying the detunings, the polariton linewidths exhibit significant motional narrowing, covering both characters mentioned above. Our analytic linewidth expressions (Eqs. 34-35) agree well with the numerical exact simulations in all the parameter regimes we explored. These results indicate that the physics of motional narrowing is adequately accounted for by the single-mode 1D HTC model. We envision that both the numerical results and the analytic polariton linewidths expression presented in this work will offer great theoretical value for providing a better understanding of the exciton-polariton motional narrowing based on the HTC model.

I. INTRODUCTION

The term *motional narrowing* is first put forward by Bloembergen, Purcell, and Pound [1–3] in the 1940s, which is a counter-intuitive phenomenon that spectral lines become sharper and narrower the more frequently the nuclear spins are disturbed in nuclear magnetic resonance (NMR) spectra. Later, this concept is used to explain the lineshapes in all facets of spectroscopy, in all research fields and across all frequency bands [4–14]. The motional narrowing effect cavity exciton-polaritons [15] had recently attracted attention, due to the fact that polariton has a much smaller effective mass and shorter lifetime compared to exciton, thus exhibiting more significant quantum mechanical effects and causes spatial averaging of disorder potential. Specifically, the disorder can be suppressed under strong light-matter coupling, reducing the width of spectral lines (which correspond to some quantum transitions). The first experimental find of cavity exciton-polariton motional narrowing effect is achieved by Whittaker *et al.* [14], where a characteristic subaverage behavior of the polariton linewidths (which means narrower than the average of the cavity and exciton linewidths) are observed. Moreover, the upper polariton (UP) and the lower polariton (LP) exhibit different narrowing behavior, that the UP is always broader than the LP. These universal behaviors observed in experiments cannot be explained by simply averaging the exciton and photon linewidths, as would be valid if both were homogeneously broadened [14, 16]. Other experimental work was quickly and extensively followed up later [17–23].

Shortly after the first experimental findings, Kinsler and Whittaker [24] provided a phenomenological explanation for the subaverage behavior. The main idea in that work was recognizing that the exciton lineshape is commonly a Gaussian, and the photon lineshape is a Lorentzian. With given widths, the convolution between a Gaussian and a Lorentzian (*i.e.*, Voigt function) has a linewidth narrower than the convolution of two Lorentzians (*i.e.*, direct average of the linewidths). However, it does not provide the scaling relation between the polariton linewidth with the number of molecules N, nor does it explain the experimentally observed asymmetry between the UP and LP linewidths. Savona *et al.* [25] proposed a microscopic model of disordered quantum wells embedded in a microcavity. By solving the nonperturbative coupled equations of motion of the exciton and cavity photon system numerically, they successfully recovered the experimental results by Whittaker *et al.* [14] in terms of motional narrowing, explaining both the subaverage behavior and why the upper UP is always broader than the LP – due to inter-branch scattering, in which the multiple scattering to all orders is emphasized [25]. Nevertheless, a lot of theoretical controversies are generated and remain unresolved [11, 25–31]. For example, it is mentioned in Ref. 25 that the motional narrowing effects are more pronounced in a 1D system than in a 2D system, while Ref. 28 made the opposite statement. And it is not clear the necessity of includ-

* wying3@ur.rochester.edu
† pengfei.huo@rochester.edu

ing the full dispersion band, as well as considering the polariton multiple scatterings. Therefore, it is of great importance to establish a minimal physical model and theory to clarify the above-mentioned ambiguities.

Recently, Climent, Subotnik, and Nitzan [31] applied the Kubo-Anderson classical stochastic theory of molecular spectral lineshape [32–34] to the case of polaritons formed in the collective strong coupling regime. By including only one cavity mode which collectively interacts with many molecules, they provided simple analytic results in the fast and slow limits of the disorder dynamics and can be evaluated numerically for the intermediate case. In particular, the polariton linewidth scales like $1/\sqrt{N}$ under the slow limit. Despite the theoretical success in Ref. 31, we want to emphasize that the Kubo-Anderson theory is classical and Markovian. It predicts that no narrowing effect can be exhibited under the fast limit [31], and does not explain the experimentally observed asymmetry between the UP and LP linewidths. Moreover, Ref. 31 focused on the resonant case and lacked the discussion for general detuned cases. With regard to these limitations, new theoretical and numerical efforts are urgently needed, in which a fully quantum mechanical description of the phonon environment should be emphasized.

In this work, we adopt the 1D Holstein-Tavis-Cummings (HTC) model [35–37] with single cavity mode to study the motional narrowing effect under a variety of different parameter regimes, based on a system-bath formalism of open quantum systems. We performed numerically exact quantum dynamics simulations using the hierarchical equations of motion (HEOM) for the linear absorption (LA) spectra of the single mode 1D HTC model. In particular, the polaron decoupling effect [35, 36] has been investigated and applied to explain the spectral linewidths narrowing phenomena [36, 38]. Our theoretical analyses reveal that in the polaron decoupling regime, the polariton linewidth scales as $1/\sqrt{N}$ under the slow limit which agrees with the Kubo-Anderson theory in Ref. 31, and scales as $1/N$ under the fast limit. Both the UP and the LP are subject to motional narrowing of the spectral response, and this effect for UP is less significant than LP due to inter-branch transitions (mainly to the dark states) that the UP branch exhibits. Moreover, we provide modified analytic expressions (Eqs. 34-35) to describe the subaverage behavior of the polariton linewidths under general detuned cases. Our analytic expressions are in excellent agreement with the results obtained from numerical exact simulations. As a consequence, our results show that a single mode 1D HTC model will be adequate to exhibit a significant motional narrowing effect featured by the subaverage behavior of the polariton linewidths for both UP and LP, without inclusion of the full dispersion band, and to exhibit the experimentally observed asymmetry between the UP and LP branches.

This paper is organized as follows. In Sec. II, we briefly review the HTC model Hamiltonian; in Sec. III, we discuss the polaron decoupling effect and its influences on the polariton linewidth, as well as the scaling relations of polariton linewidth with N under the fast and slow limits; in Sec. IV, we provide analytic linewidth expressions for LP and UP under the fast limit and the general detuned cases; in Sec. V, we present numerical exact simulations using HEOM for the polariton LA spectra and compare their linewidths with the theoretical predictions; in Sec. VI, we briefly conclude the paper. In addition, we denote the full width at half maximum (FWHM) of the peaks in LA spectra as the linewidth throughout this paper unless specified.

II. THE HOLSTEIN-TAVIS-CUMMINGS MODEL

A. Hamiltonian

We first introduce the HTC model Hamiltonian [36, 37, 39, 40] with a single cavity mode. The total Hamiltonian can be written as a system-bath form as follows

$$\hat{H}_{\mathrm{HTC}} = \hat{H}_{\mathrm{S}} + \hat{h}_{\mathrm{B}} + \hat{H}_{\mathrm{SB}}. \tag{1}$$

The system term $\hat{H}_{\mathrm{S}}$ consists of the excitonic degrees of freedom (DOF) of the molecules and the photonic DOF of the cavity and can be further expressed as [41]

$$\hat{H}_{\mathrm{S}} = \hat{H}_{\mathrm{M}} + \hat{H}_{\mathrm{cav}} + \hat{H}_{\mathrm{LM}}, \tag{2}$$

where $\hat{H}_{\mathrm{M}}$ describes the matter contribution due to the excitonic DOF, $\hat{H}_{\mathrm{cav}}$ describes the cavity radiation field, and $\hat{H}_{\mathrm{LM}}$ is the light-matter interaction term. The matter Hamiltonian $\hat{H}_{\mathrm{M}}$ describes N identical and non-interacting molecules; each molecule is modeled as an effective two-level system that represents the molecule's ground state $|g_n\rangle$ and excited state $|e_n\rangle$ (for the n_{th} molecule). The matter Hamiltonian is written as

$$\hat{H}_{\mathrm{M}} = \hbar(\omega_0 + \lambda) \sum_{n=1}^{N} \hat{\sigma}_n^+ \hat{\sigma}_n^-, \tag{3}$$

where $\hat{\sigma}_n^+ = |e_n\rangle\langle g_n|$ and $\hat{\sigma}_n^- = |g_n\rangle\langle e_n|$ are the creation and annihilation operators of the n_{th} molecule's exciton, and ω_0 is the excitation energy between the molecule's ground and excited state. The corresponding reorganization energy λ accounts for the energy shift due to exciton-phonon coupling, which is described in the system-bath interaction $\hat{H}_{\mathrm{SB}}$ (see Eq. 7). The cavity Hamiltonian $\hat{H}_{\mathrm{cav}}$ describes the quantized radiation field

$$\hat{H}_{\mathrm{cav}} = \hbar\omega_{\mathrm{c}}(\hat{a}^\dagger \hat{a} + \frac{1}{2}), \tag{4}$$

where ω_{c} is the cavity mode frequency, $\hat{a}^\dagger$ and $\hat{a}$ are the photon creation and annihilation operators of the cavity mode, respectively. Here, we consider only a single cavity mode interacting collectively with N molecules. For

the light-matter interaction term $\hat{H}_{\rm LM}$, we assume the long-wavelength approximation, that is, each molecule is coupled to the quantized radiation field with the same light-matter coupling strength $g_{\rm c}$. Under the rotating wave approximation (RWA), $\hat{H}_{\rm LM}$ is expressed as

$$\hat{H}_{\rm LM} = \hbar g_{\rm c} \sum_{n=1}^{N} \left(\hat{a}^\dagger \hat{\sigma}_n^- + \hat{a} \hat{\sigma}_n^+ \right). \tag{5}$$

Note that the system Hamiltonian $\hat{H}_{\rm S}$ in Eq. 2 is just the Tavis-Cummings model [41, 42] (with a constant energy shift λ for the exciton site energies).

The bath Hamiltonian $\hat{h}_{\rm B}$ in Eq. 1 describes the nuclear DOF, which we assume is a phonon environment that consists of a set of identical, non-interacting harmonic oscillators:

$$\hat{h}_{\rm B} = \sum_{\alpha,n} \hbar \omega_\alpha \hat{b}_{\alpha,n}^\dagger \hat{b}_{\alpha,n}, \tag{6}$$

where $\hat{b}_{\alpha,n}$, $\hat{b}_{\alpha,n}^\dagger$ are the $\alpha_{\rm th}$ bath phonon annihilation and creation operators for the $n_{\rm th}$ molecule, who satisfy the bosonic commutation relations, with ω_α the phonon frequency. The last term $\hat{H}_{\rm SB}$ in Eq. 1 characterizes the system-bath interaction which describe the exciton-phonon interaction, which we assume takes the linear form as follows

$$\hat{H}_{\rm SB} = \sum_n \hat{\sigma}_n^+ \hat{\sigma}_n^- \otimes \sum_\alpha c_\alpha (\hat{b}_{\alpha,n} + \hat{b}_{\alpha,n}^\dagger), \tag{7}$$

where $\hat{b}_{\alpha,n}$, $\hat{b}_{\alpha,n}^\dagger$ linearly couple to the n-th exciton, with c_α the coupling strength which are n-independent, *i.e.*, identical for all the molecules. To describe the interactions between the system and bath, we introduce the spectral density function, which is defined as [43, 44]

$$J(\omega) = \frac{\pi}{\hbar} \sum_\alpha c_\alpha^2 \delta(\omega - \omega_\alpha) = \frac{2\lambda \omega_f \omega}{\omega_f^2 + \omega^2}, \tag{8}$$

being identical for all excitons (for $n \in [1, N]$). We use a Drude-Lorentz form for the spectral density in our investigations, where ω_f is the bath characteristic frequency, and λ is the reorganization energy, which can also be expressed in terms of the coupling strength and the phonon frequencies as

$$\lambda = \frac{1}{\pi} \int_0^{+\infty} d\omega \, \frac{J(\omega)}{\omega} = \sum_\alpha \frac{c_\alpha^2}{\omega_\alpha}. \tag{9}$$

Note that Eq. 1 does not consider the cavity loss effects. In this work, the cavity loss is modeled through a phenomenological description [45] via the Lindblad dissipators, which is widely applied in molecular polariton dynamics simulations [46, 47], real-time simulations of linear and nonlinear spectroscopy for exciton polaritons [48, 49], photodissociation reactions [50–52], and photoinduced electron transfer reactions [53], etc. [54]. Specifically, we introduce a set of Lindblad dissipators for the photon mode time evolution as follows

$$\begin{aligned} \mathcal{L}_\Gamma \hat{O} = \Gamma_{\rm c}[1 + n(\omega_{\rm c})] \left(\hat{a} \hat{O} \hat{a}^\dagger - \frac{1}{2} \left\{ \hat{a}^\dagger \hat{a}, \hat{O} \right\} \right) \\ + \Gamma_{\rm c} n(\omega_{\rm c}) \left(\hat{a}^\dagger \hat{O} \hat{a} - \frac{1}{2} \left\{ \hat{a} \hat{a}^\dagger, \hat{O} \right\} \right), \end{aligned} \tag{10}$$

where

$$n(\omega) = 1/(e^{\beta\omega} - 1) \tag{11}$$

is the Bose-Einstein distribution function, $\beta = 1/(k_{\rm B}T)$ is the inverse temperature, and $k_{\rm B}$ is the Boltzmann constant. Further, $\Gamma_{\rm c}$ is the photon-loss rate, $\{\hat{A}, \hat{B}\} = \hat{A}\hat{B} + \hat{B}\hat{A}$ denotes the anti-commutator. The quantum dynamics of Hamiltonian in Eq. 1 with the Lindblad dissipators are simulated using mixed HEOM-Lindblad formalism [55], described in Sec. V A.

B. Polariton States and Rabi Splitting

We analyze the eigen spectrum of $\hat{H}_{\rm S}$, *i.e.*, the Tavis-Cummings model, in the ground and single excitation subspace, which is spanned by the zero photon-dressed ground state $|{\rm G}, 0\rangle$ where all the molecules are in the ground state and no photon in the cavity, one photon-dressed ground state $|{\rm G}, 1\rangle$ where all the molecules are in the ground state and one photon is in the cavity, and the single-molecule excited state $|{\rm E}_n, 0\rangle$ where all the molecules are in the ground state except for the $n_{\rm th}$ molecule. These diabatic states are defined as

$$|{\rm G}, 0\rangle = |g_1\rangle \otimes ... |g_n\rangle ... \otimes |g_N\rangle \otimes |0\rangle, \tag{12a}$$
$$|{\rm G}, 1\rangle = |g_1\rangle \otimes ... |g_n\rangle ... \otimes |g_N\rangle \otimes |1\rangle, \tag{12b}$$
$$|{\rm E}_n, 0\rangle = |g_1\rangle \otimes ... |e_n\rangle ... \otimes |g_N\rangle \otimes |0\rangle, \tag{12c}$$

where $|g_n\rangle$, $|e_n\rangle$ are the ground and first excited energy eigen states of site $n \in \{1, \cdots, N\}$, with $\hat{\sigma}_m^+ |g_n\rangle = \delta_{m,n} |e_n\rangle$ and $\hat{\sigma}_m^- |g_n\rangle = 0$. Further, $|0\rangle$, $|1\rangle$ are the zero and one photon Fock states, which are eigenstates of the bare-cavity Hamiltonian (Eq. 4). In the single excitation manifold, we also have a collective "bright" excitonic state

$$|{\rm B}\rangle = \frac{1}{\sqrt{N}} \sum_{n=1}^{N} |{\rm E}_n, 0\rangle \tag{13}$$

that couples to the $|{\rm G}, 1\rangle$ state through $\hat{H}_{\rm LM}$, generating polariton states $|\pm\rangle$ which are eigenstates of $\hat{H}_{\rm S}$. These $|\pm\rangle$ states are expressed as follows [41]

$$|+\rangle = \cos\Theta_N |{\rm B}\rangle + \sin\Theta_N |{\rm G}, 1\rangle \tag{14a}$$
$$|-\rangle = -\sin\Theta_N |{\rm B}\rangle + \cos\Theta_N |{\rm G}, 1\rangle, \tag{14b}$$

where the mixing angle is

$$\Theta_N = \frac{1}{2} \tan^{-1} \left[\frac{2\sqrt{N} g_{\rm c}}{\omega_{\rm c} - \omega_0 - \lambda} \right] \in [0, \frac{\pi}{2}), \tag{15}$$

and the corresponding energies $\omega_\pm$ of the $|\pm\rangle$ states are

$$\omega_\pm = \frac{\omega_0+\lambda+\omega_c}{2} \pm \frac{1}{2}\sqrt{(\omega_0+\lambda-\omega_c)^2+4Ng_c^2}. \quad (16)$$

One can define the collective Rabi splitting as follows

$$\Omega_R = \omega_+ - \omega_- = \sqrt{(\omega_c-\omega_0-\lambda)^2+4Ng_c^2}. \quad (17)$$

Under the resonance condition of $\omega_c = \omega_0+\lambda$, one has $\Omega_R = 2\sqrt{N}g_c$. We further denote the detuning between the cavity and the exciton as $\Delta\omega = \omega_c - (\omega_0+\lambda)$. One can alternatively use the Hopfield coefficients to represent the mixing angles, expressed as [16, 37]

$$|C|^2 = \sin^2\Theta_N = \frac{1}{2}\Big[1+\frac{\Delta\omega}{\sqrt{(\Delta\omega)^2+4Ng_c^2}}\Big], \quad (18a)$$

$$|X|^2 = \cos^2\Theta_N = \frac{1}{2}\Big[1-\frac{\Delta\omega}{\sqrt{(\Delta\omega)^2+4Ng_c^2}}\Big]. \quad (18b)$$

According to Eq. 14, the exciton fraction $|C_{ex}|^2$ for the UP and LP branches are

$$|C_{ex}|^2 \equiv \begin{cases} |X|^2 & \text{for UP,} \\ |C|^2 & \text{for LP,} \end{cases} \quad (19)$$

respectively, for a general detuning $\Delta\omega$.

When taking into account the finite lifetime of the cavity photon and the exciton, Eq. 16 is modified as [16, 37, 56]

$$\omega_\pm = \frac{\omega_0+\lambda+\omega_c+i(\Gamma_{ex}+\Gamma_c)}{2} \pm \frac{1}{2}\sqrt{[\omega_0+\lambda-\omega_c+i(\Gamma_{ex}-\Gamma_c)]^2+4Ng_c^2}. \quad (20)$$

where Γ_{ex} is the nonradiative decay rate of an exciton (or the molecular linewidth). Further, Γ_c is the cavity decay rate due to imperfect mirrors. As a linear superposition of an exciton and a photon, it has been believed that the lifetime of the polaritons is directly determined by Γ_c and Γ_{ex} as follows [16]

$$\Gamma_+ = |C|^2\Gamma_c + |X|^2\Gamma_{ex}, \quad (21a)$$

$$\Gamma_- = |X|^2\Gamma_c + |C|^2\Gamma_{ex}. \quad (21b)$$

Unfortunately, Eq. 21 contradicts the experimentally observed motional narrowing phenomena, including the subaverage trend and the asymmetric line widths between the UP and the LP branches [12, 13].

In the case of no detuning ($\Delta\omega = 0$), the Hopfield coefficients to each polariton state are both $|C|^2 = |X|^2 = 1/2$. The Rabi splitting in Eq. 17 is modified as [56] (when considering the exciton decay and cavity loss)

$$\Omega_R = \sqrt{4Ng_c^2-(\Gamma_c-\Gamma_{ex})^2}. \quad (22)$$

The Rabi splitting eventually vanishes when $\Gamma_c \gg \sqrt{N}g_c$. On the other hand, the system is in the strong coupling regime if the rate of exchange of energy between the molecules and the cavity photon is faster than the dissipation rate of the cavity photon (Γ_c) and the molecules (Γ_{ex}) [56], *i.e.*,

$$2\sqrt{N}g_c > (\Gamma_c+\Gamma_{ex})/2. \quad (23)$$

Under the strong coupling condition, one can see the LA spectra exhibiting two well-separated peaks that correspond to the upper and lower polariton states, respectively.

Furthermore, there exists $N-1$ dark states $|D_k\rangle$ expressed as follows [37, 41, 57]

$$|D_k\rangle = \frac{1}{\sqrt{N}}\sum_{n=1}^{N}\exp(-2\pi i\frac{nk}{N})|E_n,0\rangle, \quad (24)$$

where $k \in \{1,\cdots,N-1\}$. The energy of the dark states remain the same as the exciton site energy. Note that the dark states have no overlap with the collective "bright" states, and they do not participate in the interaction with the cavity mode mediated by $\hat{H}_{LM}$. They are optically dark (has no transition dipole from the ground state). Eq. 14 and Eq. 24 form the polariton basis (or the Tavis-Cummings basis [41]). Further, we introduce the following discrete Fourier transform for the bath operators [57]

$$\hat{b}_{\alpha,k} := \frac{1}{\sqrt{N}}\sum_{n=1}^{N}\exp(2\pi i\frac{nk}{N})\hat{b}_{\alpha,n}, \quad (25a)$$

$$\hat{b}^\dagger_{\alpha,k} := \frac{1}{\sqrt{N}}\sum_{n=1}^{N}\exp(-2\pi i\frac{nk}{N})\hat{b}^\dagger_{\alpha,n}. \quad (25b)$$

Under the polariton basis, the HTC Hamiltonian in Eq. 1 becomes

$$\hat{H}_S = \omega_+|+\rangle\langle+| + \omega_-|-\rangle\langle-| + (\omega_0+\lambda)\sum_{k=1}^{N-1}|D_k\rangle\langle D_k|, \quad (26a)$$

$$\hat{h}_B = \sum_{\alpha,k}\omega_\alpha\hat{b}^\dagger_{\alpha,k}\hat{b}_{\alpha,k}, \quad (26b)$$

and

$$\hat{H}_{\rm SB} = \Big[\cos^2\Theta_N|+\rangle\langle+| + \sin^2\Theta_N|-\rangle\langle-| - \frac{1}{2}\sin(2\Theta_N)\Big(|+\rangle\langle-| + |-\rangle\langle+|\Big)\Big] \otimes \sum_\alpha \frac{c_\alpha}{\sqrt{N}}(\hat{b}_{\alpha,0} + \hat{b}^\dagger_{\alpha,0})$$
$$+ \cos\Theta_N\Big[\sum_{k=1}^{N-1}|{\rm D}_k\rangle\langle+| \otimes \sum_\alpha \frac{c_\alpha}{\sqrt{N}}(\hat{b}_{\alpha,k} + \hat{b}^\dagger_{\alpha,-k}) + {\rm h.c.}\Big] - \sin\Theta_N\Big[\sum_{k=1}^{N-1}|{\rm D}_k\rangle\langle-| \otimes \sum_\alpha \frac{c_\alpha}{\sqrt{N}}(\hat{b}_{\alpha,-k} + \hat{b}^\dagger_{\alpha,k}) + {\rm h.c.}\Big]$$
$$+ \sum_{k=1}^{N-1}\sum_{j=1}^{N-1}|{\rm D}_k\rangle\langle{\rm D}_j| \otimes \sum_\alpha \frac{c_\alpha}{\sqrt{N}}(\hat{b}_{\alpha,-j+k} + \hat{b}^\dagger_{\alpha,j-k}), \tag{26c}$$

where $\hat{H}_{\rm S}$ is now diagonal. Transitions between $|+\rangle$, $|-\rangle$ and $\{|{\rm D}_k\rangle\}$ are only mediated by phonons in the bath. Note that in Eq. 26c, if the subscript is outside the range of $\{1, \cdots, N-1\}$, it can be moved back by adding or subtracting N due to the translational symmetry. For example, $\hat{b}_{\alpha,-k} \to \hat{b}_{\alpha,N-k}$.

III. POLARITON LINEWIDTH SCALING WITH N UNDER THE POLARON DECOUPLING LIMIT

A. Polaron decoupling effect

Herrera and Spano [35, 36] had shown that strong collective resonant coupling of a cavity field with N exciton transitions can effectively decouple exciton-phonon couplings in a disordered molecular ensemble. This has also been observed experimentally [38]. To be specific, the coupling strength is re-scaled as $c_\alpha/\sqrt{N}$ for both the diagonal (Holstein coupling) and off-diagonal (Peierls coupling) terms associated with the polariton states $|+\rangle$ and $|-\rangle$ as shown in Eq. 26c. In particular, under the resonance condition, the mixing angle is $\Theta_N = \pi/4$. As a result, the displacement between the $|{\rm G}, 0\rangle$ and the $|\pm\rangle$ states is given by [36] $\mathcal{R}_{\alpha,0} = R_{\alpha,0}/(2\sqrt{N})$, where $R_{\alpha,0} = \sqrt{2c_\alpha^2/\omega_\alpha^3}$ is the displacement between a given exciton state $|{\rm E}_n, 0\rangle$ and the ground state $|{\rm G}, 0\rangle$. Thus, the effective reorganization energy λ_N between the $|{\rm G}, 0\rangle$ state and the $|\pm\rangle$ states is

$$\lambda_N = \frac{1}{2}\sum_\alpha \omega_\alpha^2 \mathcal{R}_{\alpha,0}^2 = \lambda/(4N), \tag{27}$$

which is $4N$ times smaller than outside the cavity case. Intuitively, this is because when the collective Rabi oscillation period is shorter than the time scales for vibrational motion, the excitons can exchange their energy with the cavity mode many times before the nuclei have time to reorganize their configuration to the excited state potential. For large N, the reorganization energy will approach to zero, and the equilibrium positions of the polaritonic states potential and the ground state potential are aligned [35, 36].

The width of the optical lineshape (such as polariton absorption) that corresponds to $|{\rm G}, 0\rangle \to |\pm\rangle$ optical transition is contributed by both exciton and cavity broadenings. Here we consider the linear absorption (LA) spectra. A concise review for the LA spectra lineshape theory is provided in Appendix A, in which a simple two-state model is discussed.

Under the high temperature limit of $k_{\rm B}T \gg \hbar\omega_f$, we define the dimensionless parameter as follows [58]

$$\kappa_N = \Big(\frac{\hbar\omega_f^2}{2\lambda_N k_{\rm B}T}\Big)^{1/2} \propto \sqrt{N}, \tag{28}$$

where λ_N is defined in Eq. 27. By simply considering only the two polariton states (without including the dark states) coupled to a Drude-Lorentz bath [58], the polariton lineshape can be expressed analytically under two well-known limits based on κ_N, discussed below.

B. The slow limit

First, we focus on the slow limit defined as $\kappa_N \ll 1$, where the polaritons exhibit Gaussian lineshape, expressed as follows [58]

$$\mathcal{A}_N^\pm(\omega) = \frac{1}{\sqrt{2\pi\Delta_N^2}}\exp\Big[-\frac{(\omega-\omega_\pm)^2}{2\Delta_N^2}\Big], \tag{29a}$$

where the polariton frequencies $\omega_\pm$ can be found Eq. 20, and the square variance

$$\Delta_N^2 = 2\lambda_N k_{\rm B}T/\hbar \propto 1/N. \tag{29b}$$

As a result, the scaling of the polariton linewidth is $\Delta_N \propto 1/\sqrt{N}$, agreeing the Kubo-Anderson theory described in Ref. 31.

C. The fast limit

The other is the fast limit $\kappa_N \gg 1$, where the polaritons spectra exhibit a Lorentzian lineshape, expressed as follows [58]

$$\mathcal{A}_N^\pm(\omega) = \frac{1}{\pi}\frac{\Gamma_N/2}{(\omega-\omega_\pm)^2 + \Gamma_N^2/4}, \tag{30a}$$

with linewidth

$$\Gamma_N = 2\lambda_N k_B T/(\hbar\Lambda) \propto 1/N. \tag{30b}$$

As a result, the polariton linewidth scales as $1/N$ under the fast limit, which differs from the *no narrowing effect* prediction of Kubo-Anderson theory under the fast limit in Ref. 31. Note that the scaling relations with N in Eqs. 29b and 30b will not be influenced if the high temperature limit ($k_B T \gg \hbar\omega_f$) is not satisfied.

The scaling relations with N in Eqs. 29b and 30b under the slow and fast limits are the first main theoretical result of this paper. In this work, we are more interested in the fast limit because usually $N \gg 1$ in typical experimental setups, such that $\kappa_N \gg 1$. As a consequence, the polariton lineshape is described by Lorentzian (Eq. 30). We also want to emphasize that only the two polariton states are included to obtain Eqs. 29- 30. The dark states and inter-branch scattering processes have not been considered yet. This will be further discussed in the following section.

IV. A GENERAL THEORY OF POLARITON LINEWIDTH UNDER THE FAST LIMIT

A. LP linewidth

Under the strong coupling condition (Eq. 23), the polaron decoupling limit is reached around the resonance condition, where the mixing angle $\Theta_N \to \pi/4$. As a result, the polariton linewidth will become much narrower than systems outside the cavities [36, 38]. Under the fast limit, the polariton lineshape is described by Lorentzian (Eq. 30). Further consider the cavity loss with Γ_c as the (homogeneous) cavity loss rate, so that the bare photon spectral lineshape is also described by a Lorentzian. As a result, the overall LP linewidth is *additive*, reading as

$$\tilde{\Gamma}_- = \Gamma_c/2 + \Gamma_{ex}/(2N), \tag{31}$$

where a $1/N$ factor is associated to the exciton contribution Γ_{ex} due to the polaron decoupling effect, as is discussed in section III. Consequently, the LP linewidth in Eq. 31 is much narrower compared to Eq. 21 (under the resonance condition), which primarily explains the subaverage behavior of the LP linewidth in polariton motional narrowing.

On the other hand, when the cavity frequency is far detuned from the exciton energy such that $|\Delta\omega| \gg \sqrt{N} g_c$, the mixing angle $\Theta_N \to 0$ (blue-detuning limit, $\omega_c \gg \omega_x + \lambda$) or $\Theta_N \to \pi/2$ (red-detuning limit, $\omega_c \ll \omega_x + \lambda$). Under this circumstance, the time scale of Rabi oscillation is much longer than the phonon bath, which means the polaron decoupling arguments no longer hold. As a result, the system behaves like a decoupled one where the polariton states akin to pure exciton/photon states, *i.e.*,

$$\tilde{\Gamma}_- = \begin{cases} \Gamma_c & \text{for } \Theta_N \to \pi/2, \\ \Gamma_{ex} & \text{for } \Theta_N \to 0. \end{cases} \tag{32}$$

In other words, the light and matter components can be easily distinguished.

For general detuned cases with a mixing angle Θ_N, to the best of our knowledge, there is *no simple closed-form theory* to quantitatively estimate the polariton line widths. What have been widely used is an empirical linewidth expression [12–14, 29, 30]:

$$\tilde{\Gamma}_- = |X|^2\Gamma_c + \frac{|C|^4}{|X|^2} \cdot (\frac{\Gamma_{ex}}{N}), \tag{33}$$

which highlights the nonlinearity of the LP linewidth. Note that Eq. 33 recovers Eq. 32 for $\Theta_N \to \pi/2$, and Eq. 31 for $\Theta_N \to \pi/4$. Remarkably, it well captures the behavior of LP linewidth for $\pi/4 < \Theta_N < \pi/2$, as shown by Rury and co-workers [12, 13]. However, Eq. 33 does not recover Eq. 32 for the limit of $\Theta_N \to 0$ (with $|C|^2 \to 1$ and $|X|^2 \to 0$) and is unbounded, which leads to a severe overestimation of the LP linewidth for $0 < \Theta_N < \pi/4$. To solve this problem, we propose the following modification to Eq. 33 as follows

$$\tilde{\Gamma}_- = |X|^2\Gamma_c + \frac{|C|^4}{|X|^2 + \frac{|C|^4}{N}} \cdot (\frac{\Gamma_{ex}}{N}), \tag{34}$$

which preserves the boundedness and recovers Eq. 32 for $\Theta_N \to 0$.

B. Inter-branch transitions and UP linewidth

It is pointed out that inter-branch scattering (between UP and dark states) is crucial to explain the difference between the UP and LP linewidths [14, 25, 28, 59]. To be specific, the UP linewidth is usually much broader than the linewidth of the LP state, mainly due to the UP $\to$ LP and UP $\to$ dark states (DS) decay channels, which causes additional broadening to UP compared to LP. By assuming that the additional broadening effect is additive, one can express the UP linewidth by further incorporating inter-branch transitions, *i.e.*,

$$\tilde{\Gamma}_+ = \tilde{\Gamma}_+^{(0)} + \Gamma_{+\to\{D_k\}} + \Gamma_{+\to-}, \tag{35}$$

where the first term

$$\tilde{\Gamma}_+^{(0)} = |C|^2\Gamma_c + \frac{|X|^4}{|C|^2 + \frac{|X|^4}{N}} \cdot (\frac{\Gamma_{ex}}{N}) \tag{36}$$

is symmetric with Eq. 34, and the last two additional broadening terms are estimated via Fermi's golden rule (FGR) as follows [60]

$$\Gamma_{+\to-} = \frac{1}{2N} \cdot \sin^2(2\Theta_N) \cdot J(\Omega_R) \cdot [n(\Omega_R) + 1], \tag{37a}$$

$$\Gamma_{+\to\{D_k\}} = \frac{2(N-1)}{N} \cdot \cos^2\Theta_N \cdot J(\omega_+ - \omega_x - \lambda) \cdot [n(\omega_+ - \omega_x - \lambda) + 1], \tag{37b}$$

where $J(\omega)$ is defined in Eq. 8, and $n(\omega)$ is defined in Eq. 11. The detailed derivations are provided in Sec. II of the Supplementary Material. On the other hand, due to the energy differences, the scattering rate constants for LP $\to$ UP ($\Gamma_{-\to+}$) and LP $\to$ DS ($\Gamma_{-\to\{\mathrm{D}_k\}}$) are much smaller in magnitude than $\Gamma_{+\to-}$ and $\Gamma_{+\to\{\mathrm{D}_k\}}$, respectively. As a result, the LP linewidth is barely influenced by inter-branch scatterings.

The polariton linewidth expressions in Eq. 34 (for LP) and Eq. 35 (for UP) are the second main theoretical result of this paper. In the next section, we will see that they successfully describe the polariton motional narrowing phenomena and quantitatively agree well with the numerically exact simulations in all parameter regimes we explored.

V. NUMERICAL RESULTS AND DISCUSSIONS

A. Model and numerical details

In this section, we use the mixed HEOM-Lindblad formalism [55] (see Sec. I of the Supplementary Material) to simulate the LA spectra of the single mode 1D HTC model. The reduced system part is restricted in the ground and first excited manifolds under the diabatic basis (see Eq. 12), and $\hat{h}_{\mathrm{B}}$ is treated as bath DOF. We briefly summarize the main model parameters used in numerical simulations in Table I, which lead to a dimensionless parameter of $\kappa_N \approx 1.26\sqrt{N}$ (see Eq. 28), so that the bath is in the fast limit as N increases. The bath parameters lead to a bare exciton linewidth of about $\Gamma_{\mathrm{ex}} \approx 76.5$ meV. Note that under the room temperature of $T = 300$ K, the thermal energy is about $k_{\mathrm{B}}T \approx 26$ meV.

TABLE I. Parameters of the single mode 1D HTC model.

Parameter	ω_0	T	λ	ω_f
Value	2.0 eV	300 K	30 meV	24.8 meV

The LA spectra can be directly computed from the Fourier transform of the dipole-dipole correlation function according to [44, 58]

$$\mathcal{A}(\omega) \propto \int_{-\infty}^{\infty} dt\ \langle\hat{\mu}(t)\hat{\mu}(0)\rangle e^{i\omega t}, \tag{38}$$

where the dipole-dipole correlation function is defined as

$$\langle\hat{\mu}(t)\hat{\mu}(0)\rangle = \mathrm{Tr}\left[\hat{\mu}(t)\hat{\mu}(0)\hat{\rho}_{\mathrm{SS}}\right], \tag{39}$$

where $\hat{\rho}_{\mathrm{SS}}$ is the steady-state reduced density matrix (RDM) obtained using the HEOM steady-state solver [61, 62], which has significant advantages over the Krylov subspace solver or long-time propagation using RK-4 integrator. Details on the procedures of the HEOM steady-state solver can be found in Ref. 62. For all the numerical simulations, the dipole operator is expressed as $\hat{\mu} = (1/\sqrt{N})\sum_{j=1}^{N}(\hat{\sigma}_j + \hat{\sigma}_j^\dagger)$, where a $1/\sqrt{N}$ prefactor is applied for spectra intensity normalization. In addition, we set the static error tolerance for self-consistent iteration (SCI) processes as 1×10^{-5} and the hierarchy levels are all truncated automatically, which converges within just a few steps. Note that with the filtering algorithm, the numerical cost of the SCI is very low.

B. Polariton linewidth scaling with N

We first examine the effect of collective coupling to polariton linewidths due to the polaron decoupling effect. By doing so, we set the overall Rabi splitting to be much larger than the bath characteristic frequency ω_f, and for simplicity, we do not include the cavity loss ($\Gamma_{\mathrm{c}} = 0$). The cavity frequency is set to be in resonance with the exciton energy ($\omega_{\mathrm{c}} = \omega_0 + \lambda$). On the other hand, we keep the overall Rabi splitting $\Omega_{\mathrm{R}} < 400$ meV so that $\eta \equiv \Omega_{\mathrm{R}}/(2\omega_{\mathrm{c}}) < 0.1$ which does not enter into the ultrastrong coupling regime [37, 63], ensuring that the RWA is valid and the dipole self-energy (DSE) term is negligible [64]. There are two schemes to explore the polaron decoupling effect to polariton linewidths, one is fixing the single molecule coupling strength g_{c} and the other is fixing the overall Rabi splitting Ω_{R}, which does not influence the scaling relation of the polariton linewidth with N.

Fig. 1 presents the collective coupling effect of polariton spectra by varying the number of molecules N under both the fast and the slow limits under the zero detuning case. Panels (a)-(c) are the results under the fast limit with $\omega_f = 24.8$ meV. Fig. 1a presents the polariton spectra by fixing single molecule coupling strength $g_{\mathrm{c}} = 68.1$ meV and varying N. The total Rabi splitting is $\Omega_{\mathrm{R}} = 2\sqrt{N}g_{\mathrm{c}}$. One can see that as N increases, the total Rabi splitting increases. The polariton lineshape are Lorentzian-like, and the linewidth becomes narrower due to the polaron decoupling effect. Fig. 1b presents the polariton spectra by fixing the total Rabi splitting $\Omega_{\mathrm{R}} = 385.2$ meV and varying N. The single molecule coupling strength is $g_{\mathrm{c}} = \Omega_{\mathrm{R}}/(2\sqrt{N})$. As N increases, a similar linewidth narrowing phenomenon is observed, being g_{c}-independent. Moreover, the polariton peaks become asymmetric, showing an upper polariton peak broader and less pronounced than the lower one. This is attributed to the influence of the dark states (UP to dark transition). The bare-molecule spectra are also provided in both panels for comparison.

Fig. 1c further shows the polariton linewidths plotted against $1/N$, which exhibit a linear trend. The blue and red open circles are the FWHM of the LP and the UP obtained from the LA spectra computed from our HEOM simulations, respectively. The blue and red dashed lines are the corresponding linear fitting results, with the coefficient of determination $R^2 \approx 0.999$ for both LP and UP. Moreover, the slope of the fitting curve for the UP is

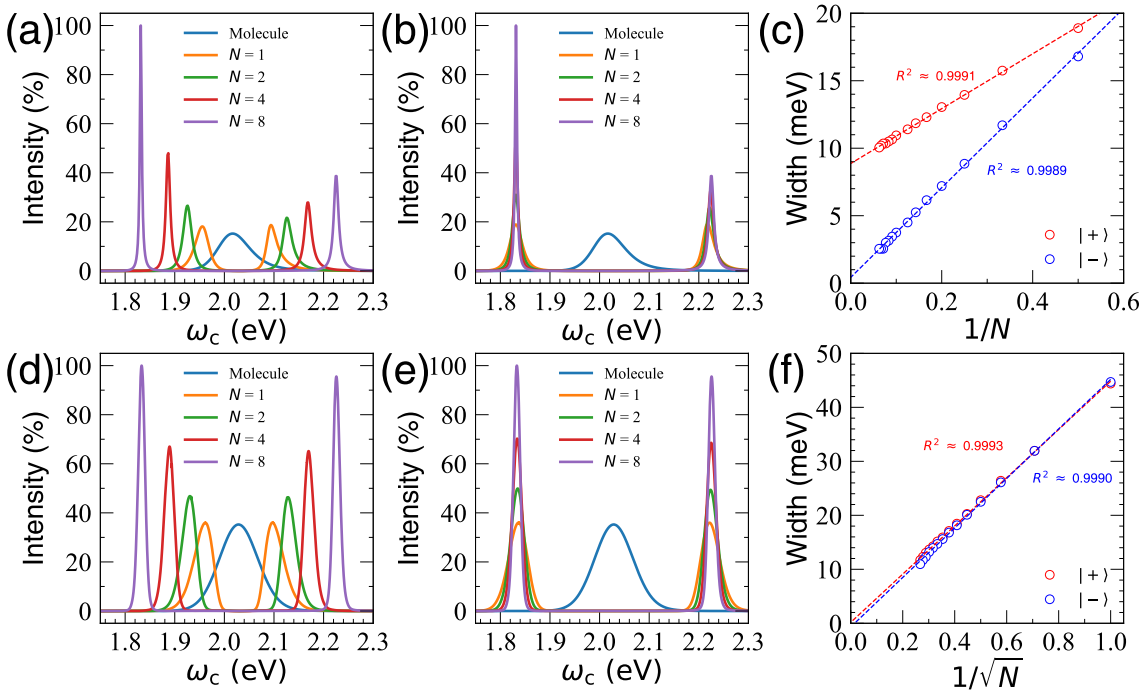

FIG. 1. Effect of collective coupling. Here $\omega_c = \omega_0 + \lambda$, the number of molecules vary from $N = 1$ to 8, no cavity loss is exerted ($\Gamma_c = 0$). (a) Fixing single molecule coupling strength $g_c = 68.1$ meV and varying N, the total Rabi splitting is $\Omega_R = 2\sqrt{N}g_c$. (b) Fixing the total Rabi splitting $\Omega_R = 385.2$ meV and varying N. The single molecule coupling strength is $g_c = \Omega_R/(2\sqrt{N})$. The bare-molecule spectra is also provided in both panels for comparison. (c) Polariton linewidths plotted against $1/N$, where the blue and red open circles are the FWHM of the LP and the UP measured from the LA spectra simulated by HEOM, respectively, and the blue and red dashed lines are the corresponding linear fitting results (with R^2 the coefficient of determination). (d)-(f) are the same as panels (a)-(c), but with $\omega_f = 2.48$ meV (slow limit), and the polariton linewidth scales as $1/\sqrt{N}$, as is shown in panel (f).

smaller than the LP, meaning the UP is less susceptible to the polaron decoupling effect than the LP. These results are in perfect accordance with the $1/N$ scaling relation predicted in Eq. 30b under the fast limit. As a corollary, under the large N limit and with the total Rabi splitting $\Omega_R \gg \Gamma_{ex}$, the exciton broadening gradually vanishes at the polariton frequencies and only the cavity broadening $\Gamma_c/2$ remains (if non-zero). As we can see from Fig. 1c that the blue dashed line extends roughly through the origin.

Fig. 1d-f further explores the collective coupling effect under the slow limit. The parameters are kept the same as panels (a)-(c) but with $\omega_f = 2.48$ meV, which results in a dimensionless parameter of $\kappa_N \approx 0.126\sqrt{N} \ll 1$ under a relatively small N (see Eq. 28). One can see that the polariton lineshape are Gaussian-like. As N increases, a similar linewidth narrowing phenomenon is observed. Moreover, the linewidth scales as $1/\sqrt{N}$ as is exhibited in panel (f), which is expected according to Eq. 29b as well as the Kubo-Anderson theory [31]. Furthermore, the lineshape is almost symmetric for the UP and the LP branches, due to much weaker inter-branch scatterings.

C. Polariton lineshape under various detunings

Next, we explore the effect of detuning on polariton lineshape. Near the resonance condition ($\omega_c = \omega_0 + \lambda$), the system enters the polaron decoupling regime which leads to linewidth narrowing, and the polariton lineshape is described by Eq. 30 under the fast limit (or Eq. 29 under the slow limit). On the other hand, in the large detuning limit ($\Theta_N \to 0$ or $\pi/2$), the system behaves like an uncoupled system where the light and matter components are well-separated. The polariton linewidths remain Γ_{ex} for the matter end and Γ_c for the photon end.

Fig. 2 presents the spectral lineshapes under different detunings near the resonance condition ($\omega_c = \omega_0 + \lambda = 2.03$ eV). In the numerical simulations, we control the parameters to always stay in the strong coupling regime (see Eq. 23 as well as Appendix B) to make the polariton peaks distinguishable from each other. Here, we fix $N = 4$ and $g_c = 68.1$ meV. The cavity frequency varies from $\omega_c = 1.83$ eV to $\omega_c = 2.23$ eV. Fig. 2a shows the results with a cavity loss rate $\Gamma_c = 44.15$ meV and $\Gamma_{ex} = 76.5$ meV. One can see that for the red-detuned cases ($\omega_c < \omega_0 + \lambda$), the LP is dominated by the photon component, with a width $\tilde{\Gamma}_- \sim \Gamma_c$, while the UP is

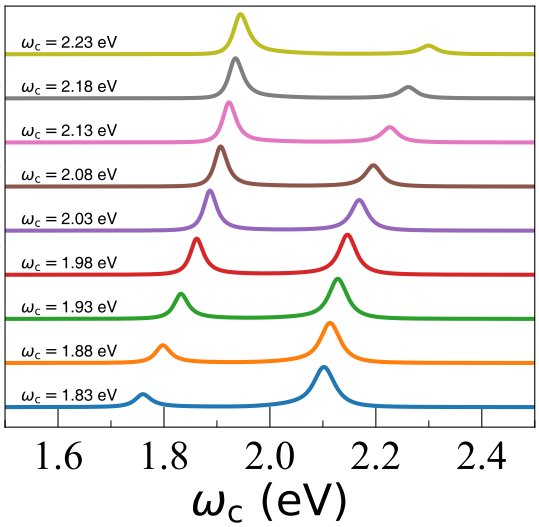

FIG. 2. Spectral lineshapes under different detunings near the resonance condition ($\omega_c \sim \omega_0 + \lambda = 2.03$ meV). Here $N = 4$, the single molecule coupling strength $g_c = 68.1$ meV, and the cavity loss rate is $\Gamma_c = 44.15$ meV.

dominated by the exciton component so that $\tilde{\Gamma}_+ \sim \Gamma_{ex}$. Moving towards the resonance condition ($\omega_c = \omega_0 + \lambda = 2.03$ meV), the polariton linewidths are narrower due to the polaron decoupling effect. Further, for the blue-detuned cases ($\omega_c > \omega_0 + \lambda$), $\tilde{\Gamma}_- \sim \Gamma_{ex}$ and $\tilde{\Gamma}_+ \sim \Gamma_c$. The FWHM of all the polariton peaks are directly obtained from the numerically simulated $\mathcal{A}_N^{\pm}(\omega)$.

D. Characters of motional narrowing

Based on the previous section, one can extract the polariton line widths with respect to different detunings. Experimentally, there are two characteristic phenomena associated with motional narrowing [14, 18]: (1) the subaverage behavior for both the UP and the LP, and (2) the asymmetric linewidths between the UP and the LP. In this section, we explore these effects via both the numerical exact simulations and the analytic linewidth expressions in Eq. 34 (for LP) and Eq. 35 (for UP).

Fig. 3 exhibits the cavity frequency (or exciton fraction) dependence of the polariton linewidths. Here we fix the single molecule coupling strength $g_c = 68.1$ meV and change the number of molecules N. The cavity loss rate is $\Gamma_c = 44.15$ meV, corresponding to a quality factor of $\mathcal{Q} = \omega_c/\Gamma_c = 45.3$ (with $\omega_c = 2.0$ eV). For all the panels (a)-(h), the HEOM results are in open circles, the analytic linewidth in Eq. 34 (for LP) and Eq. 35 (for UP) are in solid lines, and Eq. 21 are in silver dashed lines. Figs. 3a-b present the polariton linewidths (blue for the LP and red for the UP) when $N = 1$, in which panel (a) is plotted against the cavity frequency ω_c, while panel (b) is plotted against the exciton fraction $|C_{ex}|^2$ (see Eq. 19).

Fig. 3c-h are similar to panels (a)-(b), but with $N = 2, 4, 8$, respectively. One can see that for all panels, the analytic expressions agree well with the numerical exact simulations for the linewidth of both UP and LP states. And the subaverage behavior is well captured as both linewidths are lower than the silver dashed line in our simulations, but more impressively, for the analytic answer to semi-quantitatively describe them. As N increases, the subaverage behavior for the UP and the LP linewidth become more pronounced. This is because, with a larger N, λ_N is smaller (see Eq. 27) so that the exciton contribution to the linewidth becomes smaller (which scales as $1/N$ in the fast limit considered in the model here) in the polaron decoupling regime. Further, the difference between the UP and the LP linewidth becomes larger, because a larger number of dark states are presented thus more channels for inter-branch transitions. Here, the LP is generally narrower than the UP except for the $N = 1$ case (when there is no dark state). It is pointed out by Savona *et al.* [25] that in the collective strong coupling regime, the motional narrowing occurs mainly for the lower polariton. The upper polariton, on the other hand, is affected by multiple scatterings which cause additional broadening. Our results are in good agreement with the experimentally observed trends [14, 18]. On the other hand, the linewidth expression in Eq. 21 does not change with N, so that the silver dashed line remains unchanged by varying N, which means no motional narrowing. Eqs. 34-35, on the other hand, do change with N due to the polaron decoupling effect explicitly considered in these expressions. We also have results under a smaller cavity loss rate ($\Gamma_c = 8.83$ meV), see Sec. III of the Supplementary Material.

Looking into the details, one can observe from the bottom panels of Fig. 3 that both the UP and the LP linewidth exhibit a convex distribution against the exciton fraction, which is more pronounced as N increases. The analytic expression in Eq. 34 agrees nearly perfectly with the numerical exact results when $|C_{ex}| \to 0$, but becomes less accurate as $|C_{ex}| \to 1$ and as N increases, which overestimates the LP linewidth. Similarly, Eq. 35 describes the UP linewidth better for $|C_{ex}| \to 1$ than $|C_{ex}| \to 0$. Further, regarding the linewidth differences between the UP and the LP, this effect is well captured by FGR which includes only UP to dark states (as well as to LP) scattering processes. We expect that polariton multiple scatterings (which correspond to higher order processes that are beyond FGR) play a less important role for the model parameters we considered, agreeing with the conclusion by Whittaker [28]. Going beyond, we anticipate that under larger electron-phonon coupling strengths where the FGR theory starts to fail and it becomes necessary to perform nonperturbative treatments to get the correct linewidths, then polariton multiple scatterings shall become important. It is also worth mentioning that the FGR expressions in Eq. 37 work better for the negative detuned cases than the positive detuned cases [60].

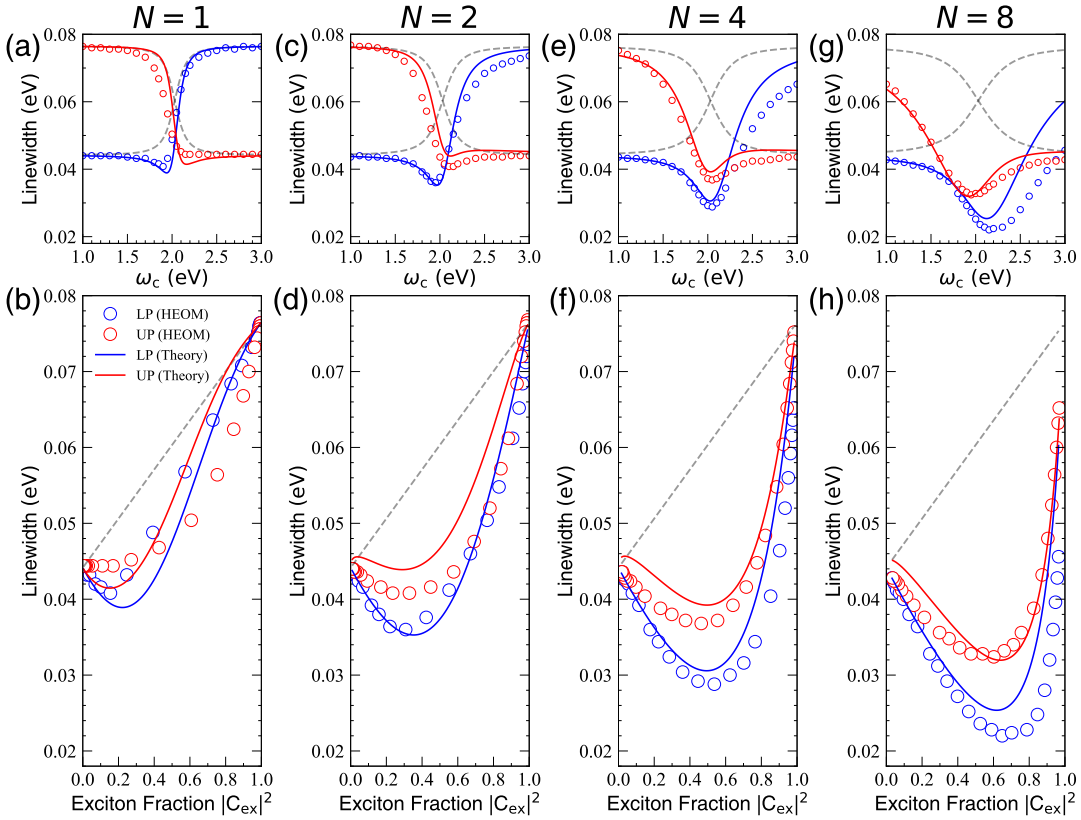

FIG. 3. Cavity frequency (or exciton fraction) dependence of the polariton linewidths. Here we fix $g_c = 68.1$ meV, and $\Gamma_c = 44.15$ meV. The HEOM results (open circles), and analytic theory in Eqs. 34-35 (solid lines) are presented, where the blue and red symbols account for the LP and the UP, respectively. The number of molecules are (a)-(b) $N = 1$; (c)-(d) $N = 2$; (e)-(f) $N = 4$; and (g)-(h) $N = 8$. The top panels are plotted against the cavity frequency ω_c, while the bottom panels are plotted against the exciton fraction $|C_{ex}|^2$ (see Eq. 19). The silver dashed line denotes the result of Eq. 21 which does not exhibit motional narrowing.

VI. CONCLUDING REMARKS

Based on the single mode 1D HTC model, we have theoretically studied the motional narrowing effect using both the analytic linewidth expressions (Eqs. 34-35) and the numerical exact simulations via HEOM. In the polaron decoupling regime, we have demonstrated that the polariton linewidth scales as $1/N$ under the fast limit, while scales as $1/\sqrt{N}$ under the slow limit, consistent with the recent work based on Kubo-Anderson theory [31]. The scaling relations are verified by numerical exact simulations. Furthermore, both the UP and the LP exhibit a subaverage behavior, and UP is usually broader than LP mainly due to inter-branch scatterings, which are the two major characteristics of the motional narrowing effect. Our results agree well with the experimental trends [12, 13]. Moreover, the analytic linewidth expressions in Eqs. 34-35 agree well with the numerical exact results in all the parameter regimes we explored. In brief, our results reveal that motional narrowing effect can be adequately described using the single mode 1D HTC model, which is also closely related to the polaron decoupling effect [35, 36].

Despite the fruitful progresses, our analytic expressions and numerical simulations have certain limitations. First, the analytic expressions are empirical and with *ad hoc* corrections. The UP linewidth expression works only when FGR is valid, which might break down in certain parameter regimes. With regard to the numerical exact simulations, the computational cost increases drastically with N, which limits us to exploring only a small number of molecules. Moreover, the HEOM method is usually restricted to certain forms of spectral density functions [65]. Future theoretical efforts are needed to address these problems.

Looking forward, the findings as well as the methods presented in this work should be very useful for providing a better understanding of the exciton-polariton motional narrowing effect [13]. A direct generalization of the current model could be extending it to 2D with many cavity modes from the full dispersion curve [37, 66], which is then referred to as the generalized Holstein-Tavis-Cummings (GHTC) model [37] and would be the closest to experimental reality [67]. A detailed study on the effect of the full cavity dispersion band and dimensionality will be extremely valuable. On the other hand,

realistic system-bath interactions are usually described by complicated spectral density functions. For example, the super-Ohmic spectral density is usually adopted for the CdSe nanoplatelet systems [40, 68, 69]. To overcome the computational difficulties, the mixed-quantum-classical (MQC) dynamics methods [49, 70, 71] could be potentially very useful. Last but not least, the polariton linewidth at general detuned cases needs to be derived basing on the first principle. For instance, using the Green's function method [14, 25, 28, 72], in which polariton multiple scatterings shall be carefully evaluated in order to obtain their contributions to the polariton linewidth. These remain to be the future work.

SUPPLEMENTARY MATERIAL

See the Supplementary Material for additional information on the hierarchical equations of motion (HEOM) as well as the mixed HEOM-Lindblad formalism; derivation for the inter-branch transition rate constants using Fermi's golden rule (FGR), where numerical illustrations are also attached; and the polariton lineshapes under a smaller cavity loss rate ($\Gamma_c = 8.83$ meV), as well as the resulting motional narrowing characters.

ACKNOWLEDGMENTS

This work was supported by the National Science Foundation Award under Grant No. CHE-2244683, as well as by the Air Force Office of Scientific Research under AFOSR Award No. FA9550-23-1-0438. W.Y. appreciates the support of the Esther M. Conwell Graduate Fellowship from the University of Rochester. P.H. appreciates the support of the Cottrell Scholar Award (a program by the Research Corporation for Science Advancement). Computing resources were provided by the Center for Integrated Research Computing (CIRC) at the University of Rochester. The authors thank Eric Koessler for valuable discussions, as well as Prof. Aaron Rury who inspired us to investigate this interesting problem.

DATA AVAILABILITY

The data that support the findings of this work are available from the corresponding author under reasonable request.

Appendix A: Theory of Linear Absorption Spectral Lineshape

Consider a two level system (with energy gap ω_0) coupled to a Drude-Lorentz bath, with spectral density

$$J(\omega) = \frac{2\lambda\Lambda\omega}{\omega^2 + \Lambda^2}, \tag{A1}$$

where λ is the reorganization energy, and Λ is the bath characteristic frequency. The LA spectra is expressed as follows [58]

$$\mathcal{A}(\omega) = \frac{1}{\pi}\mathrm{Re}\int_0^\infty dt\ \exp\left[i(\omega-\omega_0)t\right]\exp[-g(t)], \tag{A2}$$

where, $g(t) = g'(t) + ig''(t)$, with

$$g''(t) = -(\lambda/\Lambda)[\exp(-\Lambda t) + \Lambda t - 1], \tag{A3a}$$

$$g'(t) = (\lambda/\Lambda)\coth(\hbar\beta\Lambda/2)[\exp(-\Lambda t) + \Lambda t - 1] + \frac{4\lambda\Lambda}{\hbar\beta}\sum_{n=1}^{\infty}\frac{[\exp(-\nu_n t) + \nu_n t - 1]}{\nu_n(\nu_n^2 - \Lambda^2)}, \tag{A3b}$$

where $\nu_n = 2\pi n/(\hbar\beta)$ are known as the Matsubara frequencies which provide low temperature correction. Under the high-temperature limit of $k_\mathrm{B}T \gg \hbar\Lambda$, $g(t)$ can be approximated as follows

$$g(t) \approx \frac{2\lambda k_\mathrm{B}T}{\hbar\Lambda^2}[\exp(-\Lambda t) + \Lambda t - 1] - i(\lambda/\Lambda)[\exp(-\Lambda t) + \Lambda t - 1]. \tag{A4}$$

Define the following dimensionless parameter

$$\kappa = \sqrt{\frac{\hbar\Lambda^2}{2\lambda k_\mathrm{B}T}}. \tag{A5}$$

Eq. A2 has two well-known limits, one is the slow limit with $\kappa \ll 1$. As a result, $g(t) \approx \lambda k_\mathrm{B}T t^2/\hbar$, which leads to a Gaussian lineshape:

$$\mathcal{A}(\omega) = \frac{1}{\sqrt{2\pi\Delta^2}}\exp\Big[-\frac{(\omega-\omega_0)^2}{2\Delta^2}\Big], \tag{A6}$$

with $\Delta^2 = 2\lambda k_\mathrm{B}T/\hbar$. The other is the fast limit with $\kappa \gg 1$. As a result, $g(t) \approx \Gamma t - i\lambda t$, which leads to a Lorentzian lineshape:

$$\mathcal{A}(\omega) = \frac{1}{\pi}\frac{\Gamma/2}{(\omega-\omega_0)^2 + \Gamma^2/4}, \tag{A7}$$

with $\Gamma = 2\lambda k_\mathrm{B}T/(\hbar\Lambda)$.

Appendix B: The Effect of Cavity Loss Rate

In this section, we explore the effect of cavity loss rate Γ_c on polariton linewidths, which is a crucial component

for the motional narrowing. Here, the cavity loss is modeled by the Lindbladian (Eq. 10). It is straightforward to see from Eqs. 21 and 34 that under the resonance condition ($\omega_c = \omega_0 + \lambda$), cavity loss contributes to the polariton linewidths by an amount of $\Gamma_c/2$. Under the lossless limit of $\Gamma_c \to 0$, the polariton linewidths are dominated by exciton broadening, while under the lossy limit of $\Gamma_c \gg \Gamma_{ex}$, the polariton linewidths are dominated by cavity broadening.

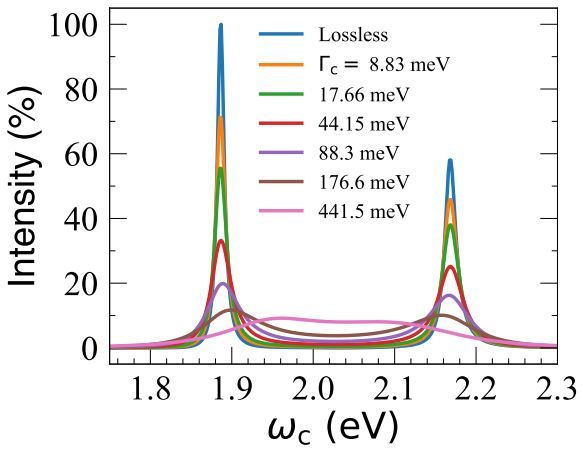

FIG. 4. Effect of cavity loss to polariton lineshapes. Here we fix $N = 4$, $g_c = 68.1$ meV, and $\omega_c = \omega_0 + \lambda$ (resonance condition). The cavity loss rate varies from $\Gamma_c = 0$ (lossless) to $\Gamma_c = 441.5$ meV.

Fig. 4 presents the effect of cavity loss on polariton lineshapes. Here, we fix $N = 4$, the single molecule coupling strength $g_c = 68.1$ meV, and the cavity frequency $\omega_c = \omega_0 + \lambda$ (resonance condition). The cavity loss rate varies from $\Gamma_c = 0$ (lossless) to $\Gamma_c = 441.5$ meV. One can see that as Γ_c increases, the polariton linewidths gradually increase while the intensity decreases, and the total Rabi splitting decreases, consistent with Eq. 22. At a very high loss rate ($\Gamma_c > \sqrt{N} g_c$), one starts to see that two polariton peaks gradually merge into one, indicating that the strong-coupling condition (Eq. 23) is no longer fulfilled. Our numerical results are in line with the previous literature results [49, 73, 74].

[1] N. Bloembergen, E. M. Purcell, and R. V. Pound, Relaxation effects in nuclear magnetic resonance absorption, Phys. Rev. **73**, 679 (1948).

[2] E. Yablonovitch, Nicolaas bloembergen (1920–2017), Nature **550**, 458 (2017).

[3] R. Kaptein, R. Boelens, and C. Luchinat, Nicolaas bloembergen: a pioneer in magnetic resonance and in maser and laser physics, J. Biomol. NMR **69**, 181 (2017).

[4] M. W. Wu and C. Z. Ning, A novel mechanism for spin dephasing due to spin-conserving scatterings, Eur. Phys. J. B **18**, 373 (2000).

[5] M. A. Brand, A. Malinowski, O. Z. Karimov, P. A. Marsden, R. T. Harley, A. J. Shields, D. Sanvitto, D. A. Ritchie, and M. Y. Simmons, Precession and motional slowing of spin evolution in a high mobility two-dimensional electron gas, Phys. Rev. Lett. **89**, 236601 (2002).

[6] C. Grimaldi, Electron spin dynamics in impure quantum wells for arbitrary spin-orbit coupling, Phys. Rev. B **72**, 075307 (2005).

[7] C. Lü, J. L. Cheng, and M. W. Wu, Hole spin dephasing in p-type semiconductor quantum wells, Phys. Rev. B **73**, 125314 (2006).

[8] W. J. H. Leyland, R. T. Harley, M. Henini, A. J. Shields, I. Farrer, and D. A. Ritchie, Oscillatory dyakonov-perel spin dynamics in two-dimensional electron gases, Phys. Rev. B **76**, 195305 (2007).

[9] J. D. Smith, R. J. Saykally, and P. L. Geissler, The effects of dissolved halide anions on hydrogen bonding in liquid water, J. Am. Chem. Soc. **129**, 13847 (2007).

[10] M. W. Wu, J. H. Jiang, and M. Q. Weng, Spin dynamics in semiconductors, Phys. Rep. **493**, 61 (2010).

[11] H.-T. Chen, Z. Zhou, M. Sukharev, J. E. Subotnik, and A. Nitzan, Interplay between disorder and collective coherent response: Superradiance and spectral motional narrowing in the time domain, Phys. Rev. A **106**, 053703 (2022).

[12] S. T. Wanasinghe, A. Gjoni, W. Burson, C. Majeski, B. Zaslona, and A. S. Rury, Motional narrowing through photonic exchange: Rational suppression of excitonic disorder from molecular cavity polariton formation, J. Phys. Chem. Lett. **15**, 2405 (2024).

[13] E. O. Odewale, S. T. Wanasinghe, and A. S. Rury, Assessing the determinants of cavity polariton relaxation using angle-resolved photoluminescence excitation spectroscopy, J. Phys. Chem. Lett. **15**, 5705 (2024).

[14] D. M. Whittaker, P. Kinsler, T. A. Fisher, M. S. Skolnick, A. Armitage, A. M. Afshar, M. D. Sturge, and J. S. Roberts, Motional narrowing in semiconductor microcavities, Phys. Rev. Lett. **77**, 4792 (1996).

[15] C. Weisbuch, M. Nishioka, A. Ishikawa, and Y. Arakawa, Observation of the coupled exciton-photon mode splitting in a semiconductor quantum microcavity, Phys. Rev. Lett. **69**, 3314 (1992).

[16] H. Deng, H. Haug, and Y. Yamamoto, Exciton-polariton bose-einstein condensation, Rev. Mod. Phys. **82**, 1489 (2010).

[17] V. Savona and C. Piermarocchi, Microcavity polaritons: Homogeneous and inhomogeneous broadening in the strong coupling regime, Phys. Status Solidi **164**, 45 (1997).

[18] C. Ell, J. Prineas, T. R. Nelson, S. Park, H. M. Gibbs, G. Khitrova, S. W. Koch, and R. Houdré, Influence of structural disorder and light coupling on the excitonic response of semiconductor microcavities, Phys. Rev. Lett. **80**, 4795 (1998).

[19] J. J. Baumberg, A. P. Heberle, A. V. Kavokin, M. R. Vladimirova, and K. Köhler, Polariton motional narrowing in semiconductor multiple quantum wells, Phys. Rev. Lett. **80**, 3567 (1998).

[20] A. V. Kavokin and J. J. Baumberg, Exciton-light coupling in quantum wells: From motional narrowing to superradiance, Phys. Rev. B **57**, R12697 (1998).

[21] P. Borri, W. Langbein, U. Woggon, J. R. Jensen, and J. M. Hvam, Microcavity polariton linewidths in the weak-disorder regime, Phys. Rev. B **63**, 035307 (2000).

[22] M. Maghrebi Melliti, R. Chtourou, J. Block, and V. Thierry-Mieg, Influence of disorder on microcavity polariton linewidths, Physica E Low Dimens. **30**, 17 (2005).

[23] F. J. Murphy, A. O. Bak, M. Matthews, E. Dupont, H. Amrania, and C. C. Phillips, Linewidth-narrowing phenomena with intersubband cavity polaritons, Phys. Rev. B **89**, 205319 (2014).

[24] P. Kinsler and D. M. Whittaker, Linewidth narrowing of polaritons, Phys. Rev. B **54**, 4988 (1996).

[25] V. Savona, C. Piermarocchi, A. Quattropani, F. Tassone, and P. Schwendimann, Microscopic theory of motional narrowing of microcavity polaritons in a disordered potential, Phys. Rev. Lett. **78**, 4470 (1997).

[26] R. Houdré, R. P. Stanley, and M. Ilegems, Vacuum-field rabi splitting in the presence of inhomogeneous broadening: Resolution of a homogeneous linewidth in an inhomogeneously broadened system, Phys. Rev. A **53**, 2711 (1996).

[27] A. V. Kavokin, Motional narrowing of inhomogeneously broadened excitons in a semiconductor microcavity: Semiclassical treatment, Phys. Rev. B **57**, 3757 (1998).

[28] D. M. Whittaker, What determines inhomogeneous linewidths in semiconductor microcavities?, Phys. Rev. Lett. **80**, 4791 (1998).

[29] M. Litinskaia and G. La Rocca, Polariton resonant scattering in semiconductor microcavities, Physics Letters A **264**, 232 (1999).

[30] M. Litinskaia and I. Kaganova, Motional narrowing in a microcavity: contribution to the lower polariton linewidth, Phys. Lett. A **275**, 292 (2000).

[31] C. Climent, J. E. Subotnik, and A. Nitzan, Kubo-anderson theory of polariton line shape, Phys. Rev. A **109**, 052809 (2024).

[32] P. W. Anderson, A mathematical model for the narrowing of spectral lines by exchange or motion, J. Phys. Soc. Jpn. **9**, 316 (1954).

[33] R. Kubo and K. Tomita, A general theory of magnetic resonance absorption, J. Phys. Soc. Jpn. **9**, 888 (1954).

[34] P. Hamm and M. Zanni, *Concepts and Methods of 2D Infrared Spectroscopy* (Cambridge University Press, 2011).

[35] F. Herrera and F. C. Spano, Cavity-controlled chemistry in molecular ensembles, Phys. Rev. Lett. **116**, 238301 (2016).

[36] F. Herrera and F. C. Spano, Theory of nanoscale organic cavities: The essential role of vibration-photon dressed states, ACS photonics **5**, 65 (2018).

[37] A. Mandal, M. A. Taylor, B. M. Weight, E. R. Koessler, X. Li, and P. Huo, Theoretical advances in polariton chemistry and molecular cavity quantum electrodynamics, Chem. Rev. **123**, 9786 (2023).

[38] S. Takahashi and K. Watanabe, Decoupling from a thermal bath via molecular polariton formation, J. Phys. Chem. Lett. **11**, 1349 (2020).

[39] M. A. Zeb, P. G. Kirton, and J. Keeling, Exact states and spectra of vibrationally dressed polaritons, ACS Photonics **5**, 249 (2018).

[40] L. Qiu, A. Mandal, O. Morshed, M. T. Meidenbauer, W. Girten, P. Huo, A. N. Vamivakas, and T. D. Krauss, Molecular polaritons generated from strong coupling between cdse nanoplatelets and a dielectric optical cavity, J. Phys. Chem. Lett. **12**, 5030 (2021).

[41] M. Tavis and F. W. Cummings, Exact solution for an n-molecule—radiation-field hamiltonian, Phys. Rev. **170**, 379 (1968).

[42] M. Tavis and F. W. Cummings, Approximate solutions for an n-molecule-radiation-field hamiltonian, Phys. Rev. **188**, 692 (1969).

[43] A. Caldeira and A. Leggett, Quantum tunnelling in a dissipative system, Ann. Phys. **149**, 374 (1983).

[44] A. Nitzan, *Chemical Dynamics in Condensed Phases* (Oxford, New York, 2006).

[45] M. O. Scully and M. S. Zubairy, *Quantum Optics* (Cambridge University Press, 1997).

[46] E. R. Koessler, A. Mandal, and P. Huo, Incorporating lindblad decay dynamics into mixed quantum-classical simulations, J. Chem. Phys. **157**, 064101 (2022).

[47] D. Hu and P. Huo, Ab initio molecular cavity quantum electrodynamics simulations using machine learning models, J. Chem. Theory Comput. **19**, 2353 (2023).

[48] I. S. Ulusoy and O. Vendrell, Dynamics and spectroscopy of molecular ensembles in a lossy microcavity, J. Chem. Phys. **153**, 044108 (2020).

[49] M. E. Mondal, E. R. Koessler, J. Provazza, A. N. Vamivakas, S. T. Cundiff, T. D. Krauss, and P. Huo, Quantum dynamics simulations of the 2D spectroscopy for exciton polaritons, J. Chem. Phys. **159**, 094102 (2023).

[50] S. Felicetti, J. Fregoni, T. Schnappinger, S. Reiter, R. de Vivie-Riedle, and J. Feist, Photoprotecting uracil by coupling with lossy nanocavities, J. Phys. Chem. Lett. **11**, 8810 (2020).

[51] E. Davidsson and M. Kowalewski, Simulating photodissociation reactions in bad cavities with the Lindblad equation, J. Chem. Phys. **153**, 234304 (2020).

[52] J. Torres-Sánchez and J. Feist, Molecular photodissociation enabled by ultrafast plasmon decay, J. Chem. Phys. **154**, 014303 (2021).

[53] D. Wellnitz, G. Pupillo, and J. Schachenmayer, A quantum optics approach to photoinduced electron transfer in

cavities, J. Chem. Phys. **154**, 054104 (2021).
[54] We note that cavity loss can also be addressed by a microscopic descriptions based on the Caldeira-Leggett system-bath model [43, 75–78], which is more fundamental and accurate and can account for non-Markovian effects [79, 80].
[55] J. Fang, Z.-H. Chen, Y. Su, Z.-F. Zhu, Y. Wang, R.-X. Xu, and Y. Yan, Coherent excitation energy transfer in model photosynthetic reaction center: Effects of non-Markovian quantum environment, J. Chem. Phys. **157**, 084119 (2022).
[56] R. Bhuyan, J. Mony, O. Kotov, G. W. Castellanos, J. Gómez Rivas, T. O. Shegai, and K. Börjesson, The rise and current status of polaritonic photochemistry and photophysics, Chem. Rev. **123**, 10877 (2023).
[57] T. E. Li, A. Nitzan, and J. E. Subotnik, Polariton relaxation under vibrational strong coupling: Comparing cavity molecular dynamics simulations against Fermi's golden rule rate, J. Chem. Phys. **156**, 10.1063/5.0079784 (2022).
[58] S. Mukamel, *Principles of Nonlinear Optical Spectroscopy* (Oxford University Press, 1995).
[59] T. Neuman and J. Aizpurua, Origin of the asymmetric light emission from molecular exciton-polaritons, Optica **5**, 1247 (2018).
[60] B. X. K. Chng, W. Ying, Y. Lai, A. N. Vamivakas, S. T. Cundiff, T. Krauss, and P. Huo, Mechanism of polariton decoherence in the collective light-matter couplings regime, ChemRxiv 10.26434/chemrxiv-2024-w70hr (2024).
[61] Y. Tanimura, Reduced hierarchy equations of motion approach with Drude plus Brownian spectral distribution: Probing electron transfer processes by means of two-dimensional correlation spectroscopy, J. Chem. Phys. **137**, 22A550 (2012).
[62] H.-D. Zhang, Q. Qiao, R.-X. Xu, X. Zheng, and Y. Yan, Efficient steady-state solver for hierarchical quantum master equations, J. Chem. Phys. **147**, 044105 (2017).
[63] A. Mandal, T. D. Krauss, and P. Huo, Polariton-mediated electron transfer via cavity quantum electrodynamics, J. Phys. Chem. B **124**, 6321 (2020).
[64] M. A. D. Taylor, A. Mandal, W. Zhou, and P. Huo, Resolution of gauge ambiguities in molecular cavity quantum electrodynamics, Phys. Rev. Lett. **125**, 123602 (2020).
[65] W. Ying, Y. Su, Z.-H. Chen, Y. Wang, and P. Huo, Spin relaxation dynamics with a continuous spin environment: the dissipaton equation of motion approach (2023), arXiv:2302.00215 [quant-ph].
[66] W. Ying, M. A. D. Taylor, and P. Huo, Resonance theory of vibrational polariton chemistry at the normal incidence, Nanophotonics **13**, 2601 (2024).
[67] We conjecture that with photon in-plane momentum, there would be more inter-branch scattering channels so that the UP would be even broader than the single mode case.
[68] F. Freire-Fernández, N. G. Sinai, M. J. H. Tan, S.-M. Park, E. Koessler, T. D. Krauss, P. Huo, and T. W. Odom, Room-temperature polariton lasing from cdse core-only nanoplatelets (2024), arXiv:2404.08395 [physics.optics].
[69] M. Amin, E. R. Koessler, O. Morshed, F. Awan, N. M. Cogan, R. Collison, T. Tumiel, W. Girten, C. S. Leiter, A. N. Vamivakas, and et al., Cavity controlled up-conversion in cdse nanoplatelet polaritons, ChemRxiv 10.26434/chemrxiv-2023-4tshv-v2 (2024).
[70] D. Bossion, W. Ying, S. N. Chowdhury, and P. Huo, Non-adiabatic mapping dynamics in the phase space of the SU(N) Lie group, J. Chem. Phys. **157**, 084105 (2022).
[71] D. Hu, W. Ying, and P. Huo, Resonance enhancement of vibrational polariton chemistry obtained from the mixed quantum-classical dynamics simulations, J. Phys. Chem. Lett. **14**, 11208 (2023).
[72] J. Yuen-Zhou and A. Koner, Linear response of molecular polaritons, J. Chem. Phys. **160**, 154107 (2024).
[73] K. Sun, C. Dou, M. F. Gelin, and Y. Zhao, Dynamics of disordered Tavis–Cummings and Holstein–Tavis–Cummings models, J. Chem. Phys. **156**, 024102 (2022).
[74] B. Gu, Toward collective chemistry by strong light-matter coupling (2023), arXiv:2306.08944 [quant-ph].
[75] S. M. Dutra and G. Nienhuis, Derivation of a hamiltonian for photon decay in a cavity, J. opt., B Quantum semiclass. opt. **2**, 584 (2000).
[76] S. M. Dutra, *Cavity Quantum Electrodynamics* (John Wiley & Sons, Ltd, 2004) pp. 255–282.
[77] L. P. Lindoy, A. Mandal, and D. R. Reichman, Quantum dynamical effects of vibrational strong coupling in chemical reactivity, Nat. Commun. **14**, 2733 (2023).
[78] W. Ying and P. Huo, Resonance theory and quantum dynamics simulations of vibrational polariton chemistry, J. Chem. Phys. **159**, 084104 (2023).
[79] I. Medina, F. J. García-Vidal, A. I. Fernández-Domínguez, and J. Feist, Few-mode field quantization of arbitrary electromagnetic spectral densities, Phys. Rev. Lett. **126**, 093601 (2021).
[80] M. Sánchez-Barquilla, F. J. García-Vidal, A. I. Fernández-Domínguez, and J. Feist, Few-mode field quantization for multiple emitters, Nanophotonics **11**, 4363 (2022).